

Self field of ac current reveals voltage–current law in type-II superconductors

E. H. Brandt,¹ G. P. Mikitik,^{1,2} and E. Zeldov³

¹*Max-Planck-Institut für Metallforschung, D-70506 Stuttgart, Germany*

²*B. Verkin Institute for Low Temperature Physics & Engineering,
Ukrainian Academy of Sciences, Kharkov 61103, Ukraine*

³*Department of Condensed Matter Physics, Weizmann Institute of Science, Rehovot 76100, Israel
(Dated: May 2, 2019)*

The distribution of ac magnetic fields in a thin superconducting strip is calculated when an ac current is applied to the sample. The edge barrier of the strip to flux penetration and exit is taken into account. The obtained formulas provide a basis to extract voltage-current characteristics in the bulk and at the edges of superconductors from the measured ac magnetic fields. Based on these results, we explain the spatial and temperature dependences of the profiles of the ac magnetic field measured in a $\text{Bi}_2\text{Sr}_2\text{CaCu}_2\text{O}_8$ strip [D.T. Fuchs et al., *Nature* **391**, 373 (1998)].

PACS numbers: 74.25.Qt, 74.25.Sv

I. INTRODUCTION

Recently a novel experimental approach for mapping the distribution of the transport current across a flat superconducting sample was developed.^{1,2} In this technique an array of microscopic Hall sensors is attached directly to the sample and the perpendicular component of the magnetic self-field generated by an ac transport current is measured at various locations across the sample. Inverting the Biot-Savart law, the distribution of the transport current across the sample can be obtained from the measured self field. It was found that in contrast to the common assumptions the transport-current distribution is highly nonuniform and varies significantly as a function of temperature T , the applied magnetic field H_a , and the phase of the vortex matter, Fig. 1. Surprisingly, over a wide range of the H - T phase diagram the current flows predominantly *at the edges* of the sample due to significant surface barriers both in high- T_c and clean low- T_c superconductors.^{1,2,3} In this situation the velocity of the vortex lattice is determined by the rate of the vortex activation over the surface barrier rather than by the bulk vortex pinning. At lower temperatures bulk vortex dynamics takes over, resulting in redistribution of the transport current; see Fig. 1. So far, however, the experimental data thus obtained were not used for quantitative study of vortex dynamics due to the absence of a detailed theoretical description.

In this paper we develop such a description. It provides the basis for the extraction of various voltage-current characteristics in the bulk and at the edges of superconductors. In Sec. II we give general formulas for the ac magnetic fields and currents, while in Secs. III-V three simple models are considered which shed light on the data presented in Fig. 1. Combinations of these models (or of more complicated models developed on the basis of the general equations of Sec. II) enable one to analyze various experimental situations in different superconductors. The obtained results show that the self-field method can be a useful tool for determination of the voltage–

current characteristics of superconductors. This development supplements the usual transport measurements and thus opens novel possibilities for a quantitative investigation of vortex dynamics.

II. GENERAL FORMULAS FOR AC MAGNETIC FIELD AND CURRENT

A. Edge barrier

Consider an infinitely long thin superconducting strip of width $2w$ and thickness $d \ll w$, filling the space $|x| \leq w$, $|y| < \infty$, $|z| \leq d/2$. Let the strip be in a constant and uniform external magnetic field H_a directed along the z axis, and let an ac current $I_a = I_{a0} \sin \omega t$ of frequency ω and of magnitude I_{a0} be applied to the sample. The current–voltage dependence for the superconducting strip in the bulk is implied to have the standard form $E = \rho(|j|)j$, with resistivity ρ being a nonlinear function of the current density j : At small current densities, $|j| < j_c$, the resistivity ρ (and thus the electric field E) is practically equal to zero; near the critical current density j_c (i.e., at $|j| \approx j_c$) the resistivity sharply increases, and it reaches a constant value ρ_H independent of j in the flux-flow regime at $|j| \gg j_c$.

In the narrow regions of the strip near its right and left edges $x = \pm w$ where the barrier for flux penetration into the strip or exit from it occurs, we shall use the current–voltage laws: $E = R_r I_r$, $E = R_l I_l$ where I_r and I_l are the currents that flow in these edge regions while R_r and R_l are the appropriate resistances per unit length in y . In other words, we model the small edge regions of the strip as “wires” with the resistances R_r and R_l . Since the edge barrier is generally different for flux entrance into the sample and for flux exit from it,⁴ these resistances are generally different, too. When $I_a > 0$, the vortices enter the strip at $x = -w$ and exits from it at $x = w$, i.e., one has $R_l = R_{en}$ and $R_r = R_{ex}$, while at $I_a < 0$ we arrive at the opposite relations: $R_l = R_{ex}$ and $R_r = R_{en}$. In general, R_{ex} and R_{en} are nonlinear functions of the

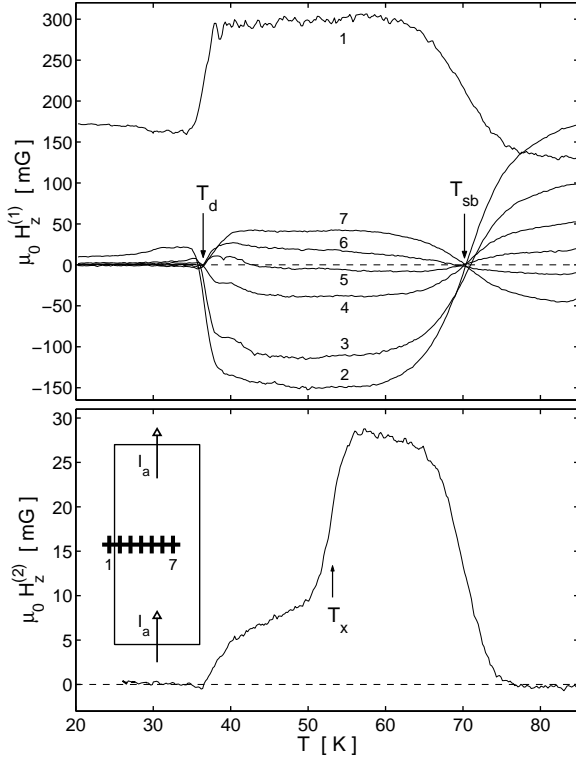


FIG. 1: Top: The temperature dependence of the in-phase part of the first harmonic of the ac self field measured by an array of 7 Hall probes at the surface of a $\text{Bi}_2\text{Sr}_2\text{CaCu}_2\text{O}_8$ strip carrying an ac current of 4 mA amplitude in a constant applied dc field of 1000 G. Bottom: The temperature dependence of the second harmonic of the ac magnetic field measured by one of the sensors at 10 mA ac current at 1000 G. Shown are also the characteristic temperatures T_d , T_{sb} , T_x . All the data from Ref. 2. The inset shows the geometry of the experiment and the positions of the sensors.

currents flowing in the appropriate edge regions.⁴

We may estimate the radius of the two edge wires from the following arguments. For a strip in a parallel magnetic field when H_a is applied along the x axis and is larger than the penetration field, the z -size of the region where the surface currents flow is less than the London penetration depth λ .⁵ It is generally believed that under condition $\lambda \ll d$, which usually holds for single crystals of high- T_c superconductors, this is also true in the considered case of a perpendicular magnetic field ($H_a \parallel z$) if H_a is higher than the lower critical field H_{c1} . In other words, one might expect that the width of the edge wires is less or of the order of λ . However, simple considerations show that this is not the case since this assumption leads to a contradiction at least for not-too-large ratio H_a/H_{c1} . Indeed, consider the situation when flux line pinning is negligible. If the edge currents flew only at $w \geq |x| \geq w - \lambda$, they would generate both H_z and H_x at least in the region $w \geq |x| \geq w - d$. This means that the flux lines are curved at such x . But without pinning and currents the curved flux lines cannot be in

equilibrium. Thus, we conclude that in a strip in a perpendicular magnetic field the edge currents flow in the whole region $w - |x| \leq d$ and probably have a complicated distribution over x and z there. With this in mind we shall assume below that the width of the edge wires is of the order of d . Note that for H_a of the order of the lower critical field H_{c1} this assumption agrees with the known result for the width of the geometrical barrier.⁶

B. Simple case

We now consider the magnetic field $H_z(x, t)$ generated by the ac current $I_a = I_{a0} \sin \omega t$. In particular, we calculate the first and the second harmonics of the ac magnetic field H_z :

$$H_z^{(1)}(x) = \frac{2}{T} \int_0^T H_z(x, t) \sin \omega t dt, \quad (1)$$

$$H_z^{(2)}(x) = \frac{2}{T} \int_0^T H_z(x, t) \cos 2\omega t dt, \quad (2)$$

where $T = 2\pi/\omega$ is the period of the oscillating ac current. (When the inductance of the strip is negligible, it follows from symmetry considerations that the first harmonic proportional to $\cos \omega t$ and the second harmonic proportional to $\sin 2\omega t$ are equal to zero.)

The total current I_a flowing in the strip at time t splits into the bulk current I_b and the edge current I_e ,

$$I_a = I_b + I_e, \quad (3)$$

where I_e consists of the left (I_l) and right (I_r) parts,

$$I_e = I_l + I_r. \quad (4)$$

If the frequency ω is not too large, the current distribution over the cross-section of the sample is uniform, and hence the sheet current in the strip $J(x)$ (i.e., the current density integrated over the thickness d of the strip) is independent of x ,

$$J(x) = \frac{I_b}{2w}. \quad (5)$$

In this case we immediately obtain

$$I_e = I_a \frac{R_b}{R_b + R_e}, \quad I_b = I_a \frac{R_e}{R_b + R_e}, \quad (6)$$

where $R_b = \rho(J/d)/2wd$ and

$$R_e = \frac{R_l R_r}{R_l + R_r} = \frac{R_{en} R_{ex}}{R_{en} + R_{ex}}. \quad (7)$$

As to I_l and I_r , one finds

$$I_l = I_e \frac{R_r}{R_l + R_r}, \quad I_r = I_e \frac{R_l}{R_l + R_r}, \quad (8)$$

with

$$R_l = R_{en}, \quad R_r = R_{ex} \quad \text{for } I_a > 0, \quad (9)$$

and

$$R_l = R_{ex}, \quad R_r = R_{en} \quad \text{for } I_a < 0. \quad (10)$$

As was mentioned above, R_b , R_{en} and R_{ex} are generally nonlinear functions of $J = I_b/2w$ and of the currents I_{en} and I_{ex} , i.e., $R_b = R_b(I_b)$, $R_{en} = R_{en}(I_{en})$ and $R_{ex} = R_{ex}(I_{ex})$, where $I_{en} = I_l$, $I_{ex} = I_r$ for $I_a > 0$, and $I_{en} = I_r$, $I_{ex} = I_l$ for $I_a < 0$. Therefore, formulas (6) - (8) are in fact equations for I_b , I_l and I_r ,

$$I_l = I_a \frac{R_r(I_r)R_b(I_b)}{[R_l(I_l) + R_r(I_r)]R_b(I_b) + R_r(I_r)R_l(I_l)}, \quad (11)$$

$$I_r = I_a \frac{R_l(I_l)R_b(I_b)}{[R_l(I_l) + R_r(I_r)]R_b(I_b) + R_r(I_r)R_l(I_l)}, \quad (12)$$

$$I_b = I_a \frac{R_r(I_r)R_l(I_l)}{[R_l(I_l) + R_r(I_r)]R_b(I_b) + R_r(I_r)R_l(I_l)}. \quad (13)$$

On determining I_l , I_r , and I_b from this set of equations, one can calculate $H_z(x, t)$ as sum of the fields of the wires and of the spatially uniform sheet current J ,

$$H_z(x, t) = \frac{1}{2\pi} \left(\frac{I_b}{2w} \ln \left| \frac{w-x}{w+x} \right| + \frac{I_r}{w-x} - \frac{I_l}{w+x} \right). \quad (14)$$

This formula together with Eqs. (11)-(13) gives H_z as a function of x and I_a , $H_z = H_z(x, I_a)$. Expressing the time t in Eqs. (1), (2) via I_a , $\sin \omega t = I_a/I_{a0} = \tilde{I}_a$, we arrive at

$$H_z^{(1)}(x) = \frac{4}{\pi} \int_0^1 H_z(x, \tilde{I}_a) \frac{\tilde{I}_a d\tilde{I}_a}{(1 - \tilde{I}_a^2)^{1/2}}, \quad (15)$$

$$H_z^{(2)}(x) = \frac{2}{\pi} \int_0^1 [H_z(x, \tilde{I}_a) + H_z(x, -\tilde{I}_a)] \frac{(1 - 2\tilde{I}_a^2)d\tilde{I}_a}{(1 - \tilde{I}_a^2)^{1/2}}. \quad (16)$$

Note that $H_z(x, -\tilde{I}_a) \neq -H_z(x, \tilde{I}_a)$ only if $R_{en} \neq R_{ex}$. Hence, the second harmonic $H_z^{(2)}(x)$ appears only when an edge barrier exists, and when this barrier leads to an asymmetry with $I_l \neq I_r$. Using formulas (3), (4), (14), expressions (15), (16) can be also rewritten in the form

$$H_z^{(1)}(x) = \frac{1}{4\pi w} \left([I_{a0} - I_e^{(1)}] \ln \left| \frac{w-x}{w+x} \right| + I_e^{(1)} \frac{2wx}{w^2 - x^2} \right), \quad (17)$$

$$H_z^{(2)}(x) = \frac{w}{2\pi(w^2 - x^2)} \Delta I_e^{(2)}, \quad (18)$$

where $I_e^{(1)}$ is the first harmonic of I_e , while $\Delta I_e^{(2)}$ is the second harmonic of $I_r - I_l$,

$$I_e^{(1)} = \frac{4}{\pi} \int_0^1 [I_r(\tilde{I}_a) + I_l(\tilde{I}_a)] \frac{\tilde{I}_a d\tilde{I}_a}{(1 - \tilde{I}_a^2)^{1/2}},$$

$$\Delta I_e^{(2)} = \frac{4}{\pi} \int_0^1 [I_r(\tilde{I}_a) - I_l(\tilde{I}_a)] \frac{(1 - 2\tilde{I}_a^2)d\tilde{I}_a}{(1 - \tilde{I}_a^2)^{1/2}}.$$

C. General case

Formulas (5)-(13) have been obtained under the assumption that the resistances are much larger than $\mu_0\omega$ (quasistatic approximation),

$$R_l, R_r, R_b \gg \mu_0\omega, \quad (19)$$

where $R_b = \rho(J/d)/2wd$. Under this assumption one can neglect the inductance of the sample, which is of the order of μ_0 (per unit length).⁷ Besides this, when $R_b \gg \mu_0\omega$, the two-dimensional penetration depth^{8,9} $\Lambda = \rho_{\text{ff}}/\mu_0\omega d$ of the ac field in the Ohmic regime is considerably larger than the width $2w$ of the strip,

$$\frac{\Lambda}{2w} = \frac{R_{\text{ff}}}{\mu_0\omega} \gg 1, \quad (20)$$

and hence, one may expect that the current distribution over the cross section of the sample is indeed uniform. Since the resistances R_l , R_r , R_b decrease with decreasing temperature T , the assumption (19) is true for not too low temperatures. We now address the general case when conditions (19) are not necessarily fulfilled.¹⁰

Let E_a be the voltage drop (per unit length) which just generates the current I_a . We now consider not only the edge regions but formally also the whole strip as a set of parallel wires. Then, we arrive at the following set of equations for the left and right edge wires and for the wires of width dx at points x ($-w < x < w$):

$$E_a = R_l I_l + L_w \dot{I}_l + L_{lr} \dot{I}_r + \int_{-w}^w dx \dot{J}(x, t) L_{xl}, \quad (21)$$

$$E_a = R_r I_r + L_w \dot{I}_r + L_{lr} \dot{I}_l + \int_{-w}^w dx \dot{J}(x, t) L_{xr}, \quad (22)$$

$$E_a = \rho_x J(x) + L_{xl} \dot{I}_l + L_{xr} \dot{I}_r + \int_{-w}^w dx' \dot{J}(x', t) L_{xx'}, \quad (23)$$

$$I_a = I_l + I_r + I_b, \quad (24)$$

where $\rho_x \equiv \rho[J(x)/d]/d$ is the sheet resistance,

$$I_b = \int_{-w}^w dx J(x, t), \quad (25)$$

the dot over currents means the time derivative, $L_{xx'} = (\mu_0/2\pi) \ln(l/|x - x'|)$ is the mutual inductance per unit length of two parallel wires of length l located at points x and x' ,⁷ $L_{xl} = (\mu_0/2\pi) \ln(l/|x + w|)$ and $L_{xr} = (\mu_0/2\pi) \ln(l/|x - w|)$ give the mutual inductances of the edge wires and that located at x , $L_{lr} = (\mu_0/2\pi) \ln(l/2w)$ is the mutual inductance of the two edge wires, and $L_w = (\mu_0/2\pi) [\ln(l/r) + 1/4]$ is the self inductance of the edge wires. Here we have assumed that both edge wires have the characteristic radius $r \sim d/2$. The magnetic field $H_z(x, t)$ is given by the Biot-Savart law

$$H_z(x, t) = \frac{1}{2\pi} \left(\frac{I_r}{w-x} - \frac{I_l}{w+x} + \int_{-w}^w \frac{J(x', t) dx'}{x' - x} \right). \quad (26)$$

Note that under conditions (19), one may keep only the first terms on the right hand sides of Eqs. (21)-(23) (omitting all time derivatives) and replace formula (25) by Eq. (5) (since the skin effect is absent). After this simplification, equations (21)- (24) and (26) are equivalent to formulas (6) - (14).

In some region above temperature T_d shown in Fig. 1, one has $R_b \gg R_e$. Thus, a situation is possible in which $R_b \gg \mu_0\omega > R_e$, and the skin effect is negligible, but one cannot omit completely the terms with the inductances in Eq. (21)-(23). In this context, it is useful to consider the case when the only assumption is the uniform distribution of the sheet current over x , i.e., the fulfilment of Eq. (5). Under this assumption Eqs. (21)- (24) reduce to a form which describes three parallel connected conductors with inductive coupling:

$$E_a = R_l \dot{I}_l + L_w \dot{I}_l + L_{lr} \dot{I}_r + L_{wb} \dot{I}_b, \quad (27)$$

$$E_a = R_r \dot{I}_r + L_w \dot{I}_r + L_{lr} \dot{I}_l + L_{wb} \dot{I}_b, \quad (28)$$

$$E_a = R_b \dot{I}_b + L_{wb} \dot{I}_l + L_{wb} \dot{I}_r + L_b \dot{I}_b, \quad (29)$$

$$I_a = I_l + I_r + I_b, \quad (30)$$

where $R_b = \rho(j)/2wd$ with $j = I_b/2wd$, $L_b = (\mu_0/2\pi)[\ln(l/2w) + 3/2]$ is the inductance of the strip for uniform current distribution in it, and $L_{wb} = (\mu_0/2\pi)[\ln(l/2w) + 1]$ is the mutual inductance of the strip and one of the edge wires. In this case Eq. (26) transforms into expression (14), and formulas (17), (18) are valid.

Equations (21)-(24) generalize the known equation for a strip with time-dependent current,^{8,9} which follows from Eq. (23) if one omits the edge-wire terms with \dot{I}_l and \dot{I}_r . Thus, the numerical procedure elaborated in Refs. 8, 9 can be applied to solve Eqs. (21)- (24) in the general case. However, in this paper we shall confine our analysis to simple models which are sufficient to understand the main features of the experimental results obtained in Refs. 1,2,3.

III. OHMIC MODEL

We begin our analysis with the simplified symmetric Ohmic model in which $R_{en} = R_{ex} = 2R_e$, and these resistances are independent of the currents $I_{en} = I_{ex}$ but depend on temperature T . We shall use a temperature dependence that satisfies the following requirement: At $T = T_c$ when the edge barrier is absent, the resistances are proportional to R_b with a geometrical factor that is the ratio of the cross-section area of the strip to the cross-section area of one of the edge wires. At lower temperatures we then take the conductance of the edge wires, $1/R_{en}$, $1/R_{ex}$, as a sum of this bulk contribution and the conductance caused by the edge barrier:

$$\frac{1}{R_{en}(T)} = \frac{1}{R_{ex}(T)} = \frac{1}{R_0(T)} + \frac{1}{2R_e^0} \left(\exp \frac{U_e(t)}{t} - 1 \right), \quad (31)$$

where $R_0(T) = (w/r)R_b(T)$, R_e^0 is some constant, $t \equiv T/T_c$, T_c is the temperature of the superconducting transition, $U_e(t)$ is the dimensionless magnitude of the edge barrier (in units of T_c), and we shall imply a linear temperature dependence of this barrier, $U_e(T) = U_e(0)(1-t)$, with some constant $U_e(0)$. The function $R_0(T)$ just gives the resistance of one of the edge wires with the edge barrier neglected ($r \sim d/2$ is the characteristic radius of the edge wire), while the second term in Eq. (31) is the edge contribution described by an Arrhenius law. We have introduced the constant -1 in the brackets to take into account that this part of the conductance vanishes at T_c . Besides this, in this Ohmic model we use $j_c(T) = 0$, and thus R_b is independent of J at all temperatures. For definiteness we take the temperature dependence of R_b in the form of an Arrhenius law, too, $R_b(T) = \rho_{\text{ff}}/2wd = R_b(T_c) \exp[-U_b(0)(1-t)/t]$, but with the constant $U_b(0)$ smaller than $U_e(0)$. The requirement $U_b(0) < U_e(0)$ emphasizes that with decreasing temperature the main contribution to the conductance of the edge wires results from the edge barrier. In the discussion below, we shall imply parameters that correspond to the experimental values:^{1,2} $I_{a0} = 4$ mA, $w = 75$ μm , $d = 10$ μm , $2w/d = 15$ ($\approx w/r$), $l = 1.5$ mm, $T_c = 88$ K, $\omega/2\pi = 73$ Hz, $R_b(T_c) \approx 6.7$ Ω/cm , yielding the large value $\Lambda/w = 2.32 \cdot 10^6$ for the two dimensional penetration depth at $T = T_c$. For definiteness, in the construction of figures we shall also take $R_e^0 = R_0(T_c)$. As to $U_e(0)$ and $U_b(0)$, we chose them so that one can reproduce the characteristic temperatures T_d and T_{sb} marked in Fig. 1.

Within this simplified model, one has $H_z^{(1)}(x) = H_z(x, t)/\sin \omega t$ and $H_z^{(2)}(x) = 0$, where under conditions (19) (at sufficiently high temperatures) $H_z(x, t)$ is given by Eq. (14), while $I_e (= 2I_l = 2I_r)$ and I_b are described by Eqs. (6). Thus, we obtain

$$H_z^{(1)}(x) = \frac{I_{a0}}{4\pi w} \left(\frac{R_e}{R_e + R_b} \ln \left| \frac{w-x}{w+x} \right| + \frac{R_b}{R_e + R_b} \frac{2wx}{w^2 - x^2} \right). \quad (32)$$

With decreasing temperature when the inequality $R_e < \mu_0\omega$ becomes valid, it is necessary to take into account the inductances of the strip and of the edge wires. In this case Eqs. (27)-(30) reduce to a set of linear equations (the time derivatives are replaced by the factor $i\omega$), and after simple calculations we find

$$2I_l = 2I_r = I_e = I_a \frac{\tilde{z}_b}{\tilde{z}_b + \tilde{z}_e}, \quad I_b = I_a \frac{\tilde{z}_e}{\tilde{z}_b + \tilde{z}_e}, \quad (33)$$

where \tilde{z}_b and \tilde{z}_e are the “effective impedances” of the strip and of the two edge wires,

$$\tilde{z}_b = R_b + i\omega(L_b - L_{wb}) = R_b + i\omega \frac{\mu_0}{4\pi}, \quad (34)$$

$$\begin{aligned} \tilde{z}_e &= R_e + i\omega \left(\frac{L_w}{2} + \frac{L_{lr}}{2} - L_{wb} \right) \\ &= R_e + i\omega \frac{\mu_0}{4\pi} \left(\ln \frac{2w}{r} - \frac{7}{4} \right). \end{aligned} \quad (35)$$

Note that even though the various inductances calculated per unit length of the strip depend logarithmically on its length l , the resulting effective impedances \tilde{z}_b , \tilde{z}_e (per unit length) are independent of l . Inserting expressions (33) in formula (14), one obtains $H_z^{(1)}(x)$. In other words, down to the temperature T_d defined in the Ohmic model by $R_b(T_d) \sim \mu_0\omega$, the first harmonic is described by formula (32) in which R_b and R_e are simply replaced by \tilde{z}_b and \tilde{z}_e . The real part of this expression gives the harmonic which is in-phase with I_a , i.e., proportional to $\sin\omega t$ like $I_a(t)$, while the imaginary part corresponds to the out-of-phase signal proportional to $\cos\omega t$.

In Fig. 2 we show the temperature dependence of $\text{Re}H_z^{(1)}$ and $\text{Im}H_z^{(1)}$ for discrete values of x similar to the locations of Hall sensors in the experiment.^{1,2} We first discuss the temperature dependence of the in-phase signal $\text{Re}H_z^{(1)}$. At temperatures near T_c , the bulk current I_b exceeds I_e since $R_b(T_c) < R_e(T_c)$, and one has an $H_z(x)$ that is characteristic of the normal state of the superconductor [the first term in Eq. (32) dominates], see Fig. 3. But the ratio of the currents I_e and I_b changes with temperature. The role of the edge current increases with decreasing T since $U_b(0) < U_e(0)$, and at a temperature $T = T_{sb} \approx 69$ K defined by $R_e(T_{sb}) = R_b(T_{sb})$ one has $I_b = I_e$, and the contributions of I_b and I_e to H_z practically compensate each other for x inside the strip. With further decrease of T , the x -dependence of H_z is mainly determined by the edge current [i.e., by the second term in Eq. (32)]. When the inductances begin to play a role at temperature $T_x \approx 46$ K defined by $R_e(T_x) \sim \mu_0\omega$ [or more exactly, by $\text{Re}\tilde{z}_e(T_x) \sim \text{Im}\tilde{z}_e(T_x)$], the impedance \tilde{z}_e saturates while \tilde{z}_b still decreases with decreasing T . As the temperature $T_d \approx 38$ K corresponding to $R_b(T_d) \sim \mu_0\omega$ is approached, the contribution of I_b to H_z begins to increase again, and the ratio of the currents, I_b/I_e tends to the constant $\ln(2w/r) - 7/4$, which is determined by the ratio of the imaginary parts of \tilde{z}_e and \tilde{z}_b . Of course, in reality at such temperatures the skin effect plays an important role, and $\text{Re}H_z^{(1)}$ tends to zero rather than to a profile determined by the above-mentioned ratio of the currents, see Fig. 2. As to the out-of-phase part of the first harmonic $\text{Im}H_z^{(1)}$, it appears only near the temperature T_x at which the inductances begin to play a role, and it differs from zero when the real and imaginary parts of the effective impedances are comparable. At still lower temperatures when R_e and R_b become negligible as compared to the imaginary parts of \tilde{z}_e and \tilde{z}_b , the out-of-phase signal vanishes again.

We now present the results for the asymmetric case when $R_{ex} \neq R_{en}$. In this situation model (31) is generalized as follows:

$$\frac{1}{R_{ex}(T)} = \frac{1}{R_0(T)} + \frac{1}{R_{ex}^0} \left(\exp \frac{U_e(t)}{t} - 1 \right),$$

$$\frac{1}{R_{en}(T)} = \frac{1}{R_0(T)} + \frac{1}{R_{en}^0} \left(\exp \frac{U_e(t)}{t} - 1 \right), \quad (36)$$

where $R_{ex}^0(T)$, $R_{en}^0(T)$ are some constants, and $R_0(T)$ is

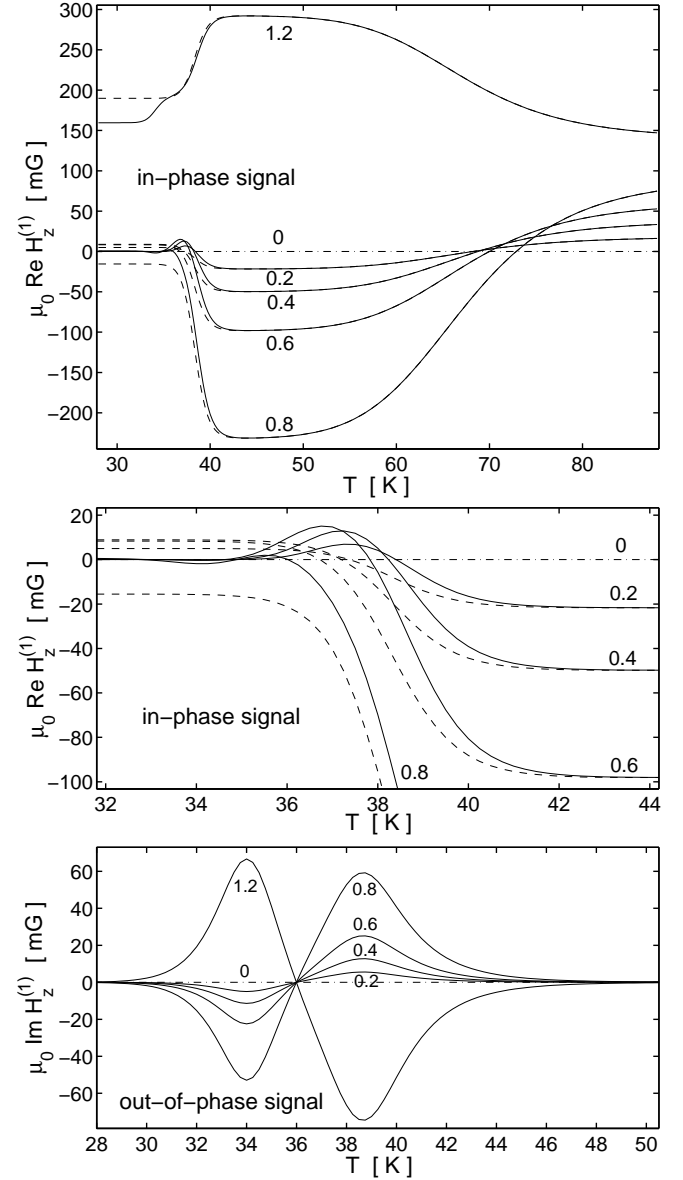


FIG. 2: The temperature dependence of the first harmonic of the ac self field which is in-phase with the applied current, $\text{Re}H_z^{(1)}$, (top) and out-of-phase with it, $\text{Im}H_z^{(1)}$, (bottom) at positions $-x/w = 1.2, 0.8, 0.6, 0.4, 0.2, 0$ on the surface of a long thin strip of width $2w$. The applied ac current is $I_a = I_{a0} \sin\omega t$. Results within the symmetric Ohmic model with $R_{en} = R_{ex}$ for $U_e(0) = 21$, $U_b(0) = 12$, $R_b(T_c) = 6.7 \Omega/\text{cm}$, $w/r = 15$, $R_e^0 = 15R_b(T_c)$, $\omega/2\pi = 73$ Hz, $T_c = 88$ K, $w = 75 \mu\text{m}$, $I_{a0} = 4$ mA. The dashed lines are the analytical results, Eq. (38), while the solid lines are numerical results from Eqs. (21)-(26) allowing for the skin effect. The solid and dashed lines coincide at $T > 42$ K, see the enlarged plot (middle). Only numerical results are shown for $\text{Im}H_z^{(1)}$ (bottom) since the analytical results, Eq. (38), neglect the skin effect and thus are applicable only at $T > 42$ K. Note the different scales of the T axis for the different plots.

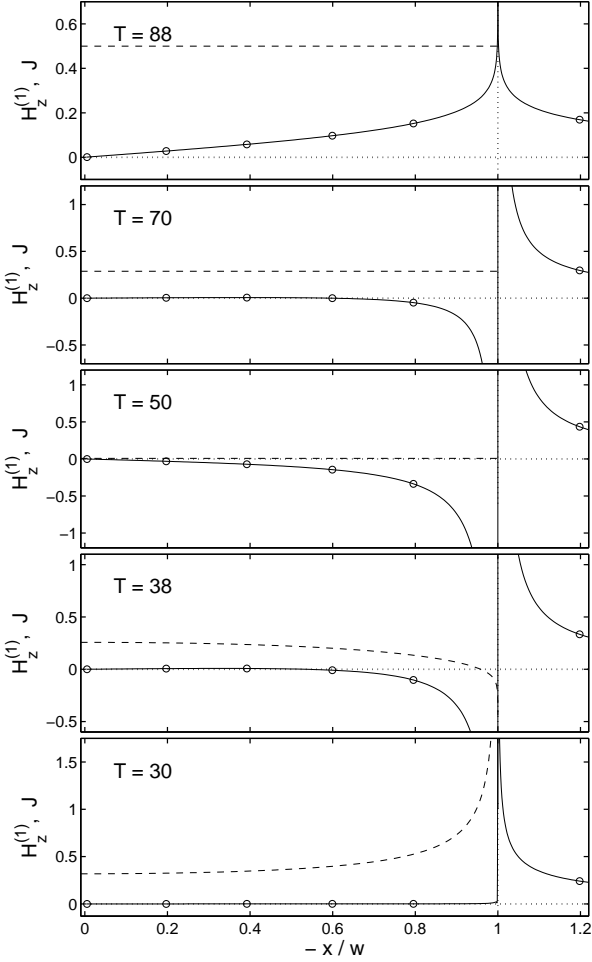


FIG. 3: The in-phase components of the magnetic field and of the sheet-current profiles, $H_z^{(1)}(x)$ (solid lines) and $J(x)$ (dashed lines), for the symmetric Ohmic model ($\eta = 0$) at temperatures $T = 85, 70, 50, 38$, and 30 K, accounting for the skin effect which occurs at $T < 42$ K, cf. Fig. 2. The parameters of the model are as in Fig. 2. The circles mark the positions of the Hall probes used in Fig. 2. Both $H_z^{(1)}$ and J are in units of I_{a0}/w . The total current in the depicted half strip is thus $1/2$, equal to the area under the dashed lines plus the (not shown) edge current at $x = w$.

the same as in Eq. (31). It is convenient to introduce the parameter

$$\eta \equiv \frac{R_{ex}^0 - R_{en}^0}{R_{ex}^0 + R_{en}^0} \quad (37)$$

which characterizes the asymmetry of the edge barrier. Then, one has

$$R_{en}^0 = 2R_e^0/(1 + \eta), \quad R_{ex}^0 = 2R_e^0/(1 - \eta),$$

where $R_e^0 = R_{en}^0 R_{ex}^0 / (R_{en}^0 + R_{ex}^0)$. We emphasize that the constant η defines the ratio $(R_{ex} - R_{en}) / (R_{ex} + R_{en})$ at sufficiently low temperatures when the conductance

$1/R_0$ is negligible in Eqs. (36), while at $T \rightarrow T_c$ the resistances R_{en} and R_{ex} tend to R_0 , the resistance of the edge wires without barrier. In other words, formulas (36) describe both the asymmetry of the edge wires at low temperatures, and the disappearance of the asymmetry when the edge barrier vanishes. Note also that $R_e = R_{ex} R_{en} / (R_{ex} + R_{en})$ is not equal to R_e^0 but approaches it with decreasing temperature.

In this asymmetric case the first harmonic becomes:

$$H_z^{(1)}(x) = \frac{I_{a0}}{4\pi w} \left(\frac{\tilde{z}_{e\eta}}{\tilde{z}_{e\eta} + \tilde{z}_b} \ln \left| \frac{w-x}{w+x} \right| + \frac{\tilde{z}_b}{\tilde{z}_{e\eta} + \tilde{z}_b} \frac{2wx}{w^2 - x^2} \right), \quad (38)$$

where

$$\tilde{z}_{e\eta} = \tilde{z}_e + \frac{(R_{ex} - R_{en})^2}{4(R_{ex} + R_{en})} \frac{ip}{1 + ip}, \quad (39)$$

\tilde{z}_e, \tilde{z}_b are given by formulas (34), (35), and

$$p \equiv \frac{2\omega(L_w - L_{lr})}{R_{ex} + R_{en}} = \frac{\mu_0\omega}{\pi(R_{ex} + R_{en})} \left(\ln \frac{2w}{r} + \frac{1}{4} \right). \quad (40)$$

This p characterizes the relative contribution of the inductance of the edge wires to their effective impedance \tilde{z}_e . Analysis of formulas (38)-(40) shows that the parameter η practically has no effect on $H_z^{(1)}$ within the considered Ohmic model, and hence the first harmonic in the asymmetric case, in fact, coincides with the harmonic in the symmetric case of $\eta = 0$. However, for the case $\eta \neq 0$ the second harmonic $H_z^{(2)}$ appears. This $H_z^{(2)}(x)$, Eq. (18), is

$$H_z^{(2)}(x) = \frac{2I_{a0}}{3\pi^2} \frac{w}{w^2 - x^2} \frac{(R_{ex} - R_{en})}{(R_{ex} + R_{en})} \frac{\tilde{z}_b}{\tilde{z}_b + \tilde{z}_{e\eta}} \frac{1}{1 + ip}. \quad (41)$$

The real part of this expression gives the harmonic proportional to $\cos 2\omega t$, and its imaginary part to $\sin 2\omega t$. In Fig. 4 we show the temperature dependence of $|H_z^{(2)}|$ at $x = 0.7w$. At temperatures near T_x introduced by $\text{Re}\tilde{z}_e(T_x) \sim \text{Im}\tilde{z}_e(T_x)$, one has $p(T_x) \sim 1$, the amplitude of the second harmonic begins to decrease with decreasing T and becomes small even at temperatures above T_d if $R_b(T_x) \gg \mu_0\omega$. Of course, at temperatures when $R_b(T) \sim \mu_0\omega$, the second harmonic $H_z^{(2)}$ vanishes in any case due to the skin effect.

We emphasize that the formulas of this section are valid not only for the model dependences (31) or (36) used here but also for any functions $R_b(T)$, $R_{en}(T)$, $R_{ex}(T)$. Thus, one can obtain some information on these functions fitting the theoretical dependences of $H_z^{(1)}(T)$ and $H_z^{(2)}(T)$ to appropriate experimental data. Independent information on the functions $R_b(T)$, $R_e(T)$ for each specific sample can be also obtained from usual transport measurements.¹¹ Beside this, some data on this subject can be extracted from frequency dependences of $H_z^{(1)}(T)$ and $H_z^{(2)}(T)$ since these harmonics are functions of the combinations $(R_b/\mu_0\omega)$, $(R_{en}/\mu_0\omega)$, $(R_{ex}/\mu_0\omega)$. In the

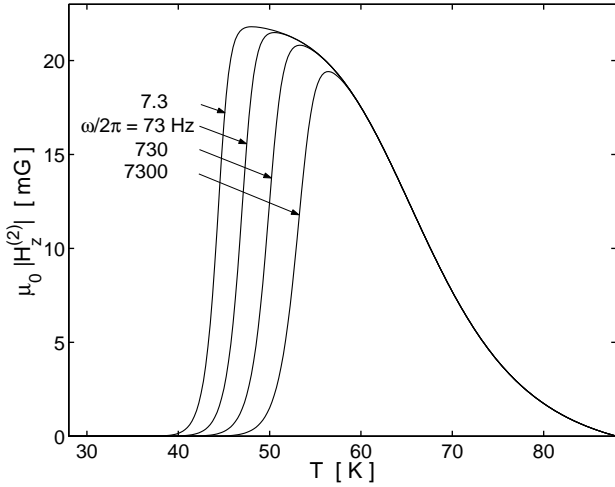


FIG. 4: The temperature dependence of the magnitude of the second harmonic of the ac self field, $|H_z^{(2)}|$, at position $|x/w| = 0.7$ on the surface of a long thin strip of width $2w$ with applied ac current $I_a = I_{a0} \sin \omega t$. Results within the Ohmic model, Eq. (41), for the same parameters as in Fig. 2 but with asymmetry $\eta = 0.1$ and amplitude $I_{a0} = 10$ mA (line at $\omega/2\pi = 73$ Hz). The other lines are for different frequencies.

framework of our model (36), if one changes the frequency ω from ω_1 to ω_2 , the temperature dependence of the first harmonic changes only near T_d , while the temperature dependence of the second harmonic changes in the vicinity of T_x (the appropriate parts of these dependences shift to higher temperatures with increasing ω), see, e.g., Fig. 4. The shifts of the temperatures T_d and T_x are

$$\begin{aligned} T_d(\omega_2) - T_d(\omega_1) &\approx \frac{T_d^2}{U_b(0)T_c} \ln \left(\frac{\omega_2}{\omega_1} \right), \\ T_x(\omega_2) - T_x(\omega_1) &\approx \frac{T_x^2}{U_e(0)T_c} \ln \left(\frac{\omega_2}{\omega_1} \right), \end{aligned} \quad (42)$$

and they give information on $U_b(0)$ and $U_e(0)$.

We now briefly discuss the applicability of the considered temperature dependences of R_e and R_b to BSCCO samples. The experimental data on resistance of BSCCO strips obtained from usual transport measurements are well approximated by an Arrhenius law.^{11,12,13,14} In principle, parameters $U_e(0)$ and R_e^0 can be found from these data, while $U_b(0)$ can be estimated in similar experiments with wide samples.¹¹ In particular, in Ref. 11 it was found that $U_e(0) \approx 12$ for the same crystal as in Fig. 2, and it was estimated that $U_b(0) \leq 8$. Both these values are noticeably less than those used in the construction of Figs. 2 and 4. The latter values were chosen such that one can reproduce the experimental T_d and T_{sb} . In Figs. 2 and 4 we have also used the specific value of R_e^0 , $R_e^0 = R_0(T_c)$. Other choices of the parameter R_e^0 enable one, in principle, to use a smaller value of $U_e(0) - U_b(0)$, but do not provide the coincidence of both $U_e(0)$ and $U_b(0)$ with their experimental values [in the Ohmic model the value

of $U_b(0) \approx 12$ is fixed by the condition $R_b(T_d) \approx \mu_0 \omega$].¹⁵ Such disagreement seems to signal that the Ohmic model does not work in the whole interval from T_d to T_c for the BSCCO crystals.

Finally, we note two characteristic features of the Ohmic model studied here. First, if the magnetic field is measured in units of I_{a0}/w , the first and the second harmonics are independent of the amplitude I_{a0} of the applied current. In particular, the characteristic temperatures T_d , T_{sb} , T_x do not shift with a change of I_{a0} . This scaling property may be used in experiments to find the temperature regions where the Ohmic model is applicable. Second, the resistance of the strip, $R = R_b R_e / (R_b + R_e)$ is also independent of I_{a0} and can be used for the same aim as well.

IV. MODEL OF NONLINEAR $R_e(I_e)$

The data of Ref. 3 obtained for different currents I_{a0} show that at least for some superconductors R_e cannot be considered as a quantity that is independent of I_e for all temperatures. To get an insight into this problem, we shall now analyze a simple model of nonlinear dependence $R_e(I_e)$ and show that this nonlinearity can provide an alternative description of the experimental temperature dependences of $H_z^{(1)}$ and $H_z^{(2)}$ near T_{sb} . In principle, this and a similar nonlinear model for $R_b(I_b)$ near T_d enable one to describe the experimental data on $H_z^{(1)}$ and $H_z^{(2)}$ with realistic values of $U_e(0)$ and $U_b(0)$.

We shall consider the following simple model dependences $R_{en}(I_{en})$ and $R_{ex}(I_{ex})$ for the flux entrance into the strip and the flux exit from it: When I_{en} (or I_{ex}) exceeds the critical current I_{en}^c (I_{ex}^c) for flux entrance (exit), the resistivity of the edge wire is the same as in the bulk of the strip, and hence the resistance of the edge wire $R_{en}(I_{en})$ [$R_{ex}(I_{ex})$] coincides with $R_0 = (w/r)R_b$. At $I_{en} = I_{en}^c$ ($I_{ex} = I_{ex}^c$) the resistance sharply drops down to a value R_{en} (R_{ex}) which is independent of the current I_{en} (I_{ex}) for $I_{en} < I_{en}^c$ ($I_{ex} < I_{ex}^c$), i.e., one has

$$\begin{aligned} R_{en}(I_{en}) &= R_0 \quad \text{for } I_{en} > I_{en}^c, \\ R_{en}(I_{en}) &= R_{en} \quad \text{for } I_{en} < I_{en}^c, \end{aligned} \quad (43)$$

and

$$\begin{aligned} R_{ex}(I_{ex}) &= R_0 \quad \text{for } I_{ex} > I_{ex}^c, \\ R_{ex}(I_{ex}) &= R_{ex} \quad \text{for } I_{ex} < I_{ex}^c. \end{aligned} \quad (44)$$

In other words, we replace the complicated nonlinear dependence of the edge barrier on the current flowing in the edge region⁴ by a sharp jump of the appropriate resistance. Although with the equations of Sec. II, the currents and magnetic field can be found for any realistic dependences $R_{en}(I_{en})$ and $R_{ex}(I_{ex})$, within this simple model the calculations can be carried out analytically. This enables one to get insight into situations with various relations between the edge critical currents I_{en}^c , I_{ex}^c and the resistances R_{en} , R_{ex} .

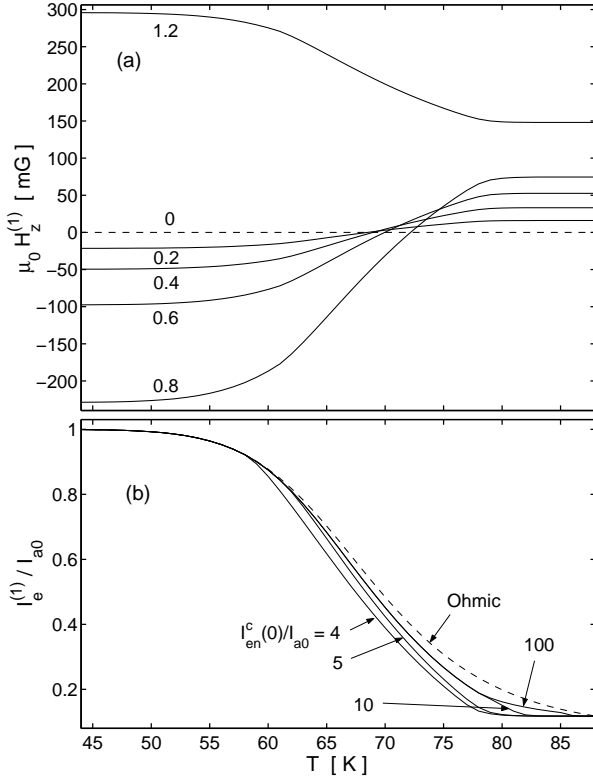


FIG. 5: Top: Temperature dependence of the first harmonic $H_z^{(1)}$ of the ac self field at positions $x/w = -1.2, -0.8, -0.6, -0.4, -0.2, 0$ on the surface of a long thin strip of width $2w$ with applied current $I_a = I_{a0} \sin \omega t$. Results within the nonlinear R_e -model for the same parameters as in Fig. 2 (symmetric case, $\eta = 0$) but with $U_e(0) = 12$, $U_b(0) = 2$, $I_{en}^c(0)/I_{a0} = I_{ex}^c(0)/I_{a0} = 4$. Assumed was $I_{en}^c(T)/I_{en}^c(0) = I_{ex}^c(T)/I_{ex}^c(0) = (1-t)^2$ where $t \equiv T/T_c$. Bottom: Temperature dependence of the first harmonic $I_e^{(1)}$ of the edge current. The parameters are the same as in the top panel but $I_{en}^c(0)/I_{a0} = 4$ (symmetric case), 5, 10, 100. If η differs from zero, the curves remain practically unchanged for $\eta < 0.3$. For comparison, the dashed line shows $I_e^{(1)}(T)$ for the symmetric Ohmic model with parameters of Fig. 2.

Let us specify the details of this model. With decreasing temperature the currents I_{en}^c and I_{ex}^c increase, and for definiteness we take $I_{en}^c = I_{en}^c(0)(1-t)^2$, $I_{ex}^c = I_{ex}^c(0)(1-t)^2$ where $t \equiv T/T_c$ (such temperature dependence of $I_{en}^c + I_{ex}^c$ was obtained in Ref. 4). We also imply that near the temperature T_{sb} these critical currents of the edge wires become larger than the amplitude of the applied current I_{a0} , and thus the drop of edge-wire resistances occurs at sufficiently high temperatures where conditions (19) are true, and so the inductances and the skin effect are ignored below. As to R_{en} , R_{ex} and R_b , we choose the same expressions for them as in the Ohmic model, but now we use $U_e(0) \approx 12$ and $U_b(0) \approx 2$ (in units of T_c), which are essentially less than those used in Sec. III.

To find the first and second harmonics of H_z , one should solve Eqs. (11)-(13) and find the currents I_l , I_r ,

and I_b as functions of I_a . From these currents, one calculates $H_z^{(1)}$, $H_z^{(2)}$ using formulas (17)-(18). Within the above simple model, these calculations can be done analytically. For example, in the symmetric case when $\eta = 0$ and $I_{en}^c = I_{ex}^c \equiv I_e^c/2$, one has formulas (6) for I_b and $I_e = 2I_l = 2I_r$ at $I_a \leq I_1 \equiv I_e^c \cdot (R_b + R_e)/R_b$ where R_b and $R_e = R_{en}R_{ex}/(R_{en} + R_{ex})$ are independent of I_b and I_e . In the interval $I_1 \leq I_a \leq I_2 \equiv I_e^c \cdot (1 + w/2r)$ we find $I_e = I_e^c$, $I_b = I_a - I_e^c$, while at $I_2 \leq I_a$ equations (11)-(13) yield

$$I_e = I_a \frac{R_b}{R_b + 0.5R_0} = I_a \cdot \left(1 + \frac{w}{2r}\right)^{-1},$$

$$I_b = I_a \frac{0.5R_0}{R_b + 0.5R_0} = I_a \frac{w}{2r} \left(1 + \frac{w}{2r}\right)^{-1}. \quad (45)$$

Using these formulas, we find the following expression for the first harmonic of I_e :

$$I_e^{(1)} = \frac{2I_{a0}}{\pi} \frac{R_b}{R_b + R_e} \left(\phi_1 - \frac{\sin 2\phi_1}{2} \right) + \frac{4I_e^c}{\pi} (\cos \phi_1 - \cos \phi_2) + \frac{2I_{a0}}{\pi} \left(\frac{\pi}{2} - \phi_2 + \frac{\sin 2\phi_2}{2} \right) \left(1 + \frac{w}{2r}\right)^{-1}, \quad (46)$$

where $\phi_1 \equiv \min(\arcsin[I_1/I_{a0}], \pi/2)$ and $\phi_2 \equiv \min(\arcsin[I_2/I_{a0}], \pi/2)$. Inserting Eq. (46) into formula (17), we obtain $H_z^{(1)}(x)$. The second harmonic of H_z in the symmetric case is equal to zero. In Appendix A we present the first and the second harmonics of H_z in the asymmetric case when $\eta \neq 0$, $I_{en}^c \neq I_{ex}^c$. Note that within this nonlinear R_e model the characteristic temperature T_{sb} is still defined by the condition $I_e^{(1)} = I_{a0}/2$ as in the Ohmic model.

In Fig. 5 we show the first harmonics $H_z^{(1)}$ of $H_z(t)$ calculated within this nonlinear R_e model. The temperature dependence of the first harmonic is qualitatively similar to that of Fig. 2, and with increasing asymmetry of the edge barrier it does not change essentially. On the other hand, the second harmonic $H_z^{(2)}$ is highly sensitive to the asymmetry, see Fig. 6. Figure 6 shows both the change of $H_z^{(2)}$ with $I_{en}^c(0)/I_{ex}^c(0)$ at fixed η and its change with η at fixed $I_{en}^c(0)/I_{ex}^c(0)$. Interestingly, the temperature dependence of $H_z^{(2)}$ is nonmonotonic and looks qualitatively similar to that of Fig. 4. But now the temperature where $H_z^{(2)}(T)$ sharply decreases is due to the temperature T_1 of Appendix A at which some characteristic current of the edge barrier becomes larger than I_{a0} . This temperature T_1 is independent of ω within our nonlinear R_e model. At temperatures $T \leq T_1$ during the whole period of the ac field, the currents flowing in the edge wires are less than the appropriate critical currents I_{en}^c , I_{ex}^c , the strip is in the Ohmic regime, and $H_z^{(1)}(T)$ and $H_z^{(2)}(T)$ obtained from the formulas of Appendix A coincide with expressions (38) and (41) if one neglects the inductive terms proportional to $\mu_0\omega$ in these expressions. This coincidence permits one to combine this nonlinear model with the Ohmic model of Sec. III and thus to obtain continuous curves in the entire temperature region.

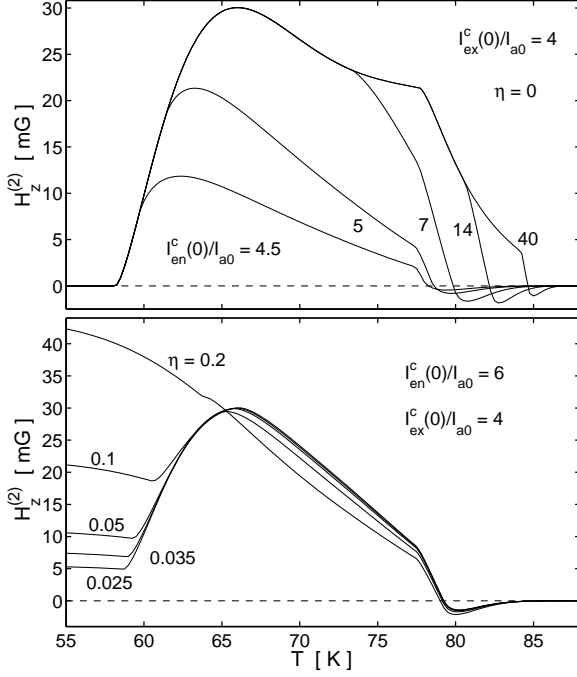


FIG. 6: The temperature dependence of the second harmonic of the ac field defined by Eq. (2) at $|x/w| = 0.7$ within the nonlinear R_e model, Eqs. (18), (A2). The parameters are the same as in Fig. 2 but with $U_e(0) = 12$, $U_b(0) = 2$, and besides this $I_{ex}^c(0)/I_{a0} = 4$. The top part shows the second harmonic at fixed $\eta = 0$ for different $I_{en}^c(0)/I_{a0} = 4.5, 5, 7, 14, 40$, while the bottom part gives this harmonic at fixed $I_{en}^c(0)/I_{a0} = 6$ but for different asymmetry $\eta = 0.025, 0.035, 0.05, 0.1, 0.2$. Note that $H_z^{(2)}(T)$ for $\eta \neq 0$ does not reach zero after its drop in the vicinity of 60 K.

Interestingly, when T is larger than the temperature T_4 of Appendix A, the maximum currents in the edge wires exceed I_{en}^c and I_{ex}^c , and the strip is in the flux-flow regime during some part of the ac period. In Fig. 6 this temperature T_4 corresponds to the point where $H_z^{(2)}(T)$ crosses zero (i.e., $T_4 \approx 78$ K in Fig. 6b).

V. MODEL OF NONLINEAR $R_b(I_b)$

As was mentioned above, in the Ohmic model below a temperature T_d defined by the condition $R_b(T_d) \sim \mu_0\omega$, the skin effect occurs, which means the perpendicular ac magnetic field H_z is expelled from the strip. However, there is another reason for this field to be expelled from the superconductor. Indeed, if the ac current flowing in the bulk is smaller than the critical current $I_c = 2wdj_c$ of the strip, the ac field cannot penetrate completely into the sample. Thus, a finite I_c and its increase with decreasing temperature can, in principle, explain the existence of the temperature T_d in Fig. 1, below which H_z is zero in the strip and at its surface. To describe this, we now consider a nonlinear R_b model in which the critical current density j_c is not equal to zero, and the resistivity

ρ depends on the current density j . We shall analyze the following model current-voltage dependence:

$$E = \rho(j)j = \rho_{\text{ff}} \frac{j j_c \epsilon(j)}{j + j_c \epsilon(j)}, \quad (47)$$

where

$$\epsilon(j) = 2e^{-U_0/T} \sinh\left(\frac{j}{j_c} \frac{U_0}{T}\right), \quad (48)$$

and j_c and the effective depth of flux-pinning well U_0 are some decreasing functions of T . Let us consider the case $U_0/T \gg 1$. Then, at $j > j_c$ one has $\epsilon(j) \gg j/j_c$, and thus $\rho(j) = \rho_{\text{ff}}$, while at $j < j_c$ the quantity $\epsilon(j)$ is small, $\epsilon(j) \ll j/j_c$, and we arrive at $\rho(j)j = \rho_{\text{ff}} j_c \epsilon(j) \ll \rho_{\text{ff}} j$.¹⁶ Thus, equations (47), (48) lead to a sharp jump of resistivity at $j = j_c$ that is characteristic for the critical state model. In analytical calculations we shall simplify the model dependence further, putting

$$\begin{aligned} \rho(j) &= \rho_{\text{ff}} & \text{for } j > j_c, \\ \rho(j) &= 0 & \text{for } j < j_c. \end{aligned} \quad (49)$$

As to the flux-flow resistivity ρ_{ff} , for definiteness we shall imply the same temperature dependence as in Secs. III and IV, $\rho_{\text{ff}}(T) = \rho_{\text{ff}}(T_c) \exp[-U_b(0)(1 - t)/t]$, where $U_b(0)$ is a dimensionless constant and $t \equiv T/T_c$. Since in this section we are mainly interested in understanding the effect of nonlinear $R_b(I_b)$ on the first harmonic of the ac field near T_d , we assume that near T_d one has $R_{\text{ff}} = \rho_{\text{ff}}/2wd \gg \mu_0\omega$, R_e , and the resistances $R_{en} = R_{ex} = 2R_e$ are independent of $I_{en} = I_{ex}$ (i.e., we treat only the symmetric situation and imply that the skin effect occurs sufficiently below T_d). The temperature dependence of the critical current $I_c = 2wdj_c$ is assumed to be a monotonically decreasing function. From our analysis it will be clear that this dependence plays the most important role in the vicinity of the temperature T_j at which $I_c(T)$ reaches I_{a0} , and so we may use the following representation of $I_c(T)$:

$$I_c(T) = I_{a0} \left[\frac{T_c - T}{T_c - T_j} \right]^n, \quad (50)$$

where n is some exponent. Note that in this representation a change of I_{a0} requires a change of T_j such that $I_c(T)$ remains unchanged.

Let us first show that at $I_{a0} \gg I_c = 2wdj_c$ our nonlinear R_b model reduces to the Ohmic model considered in Sec. III. This situation always occurs at sufficiently high temperatures when I_c is small. The nonlinearity of $R_b(I_b)$ gives only small corrections to the Ohmic results, and these corrections can be calculated analytically. Indeed, at times t when $I_b(t) > I_c$, the Ohmic model is applicable, and we have

$$I_b = I_{b0} \sin(\omega t + \varphi_b), \quad I_e = I_{e0} \sin(\omega t + \varphi_e) \quad (51)$$

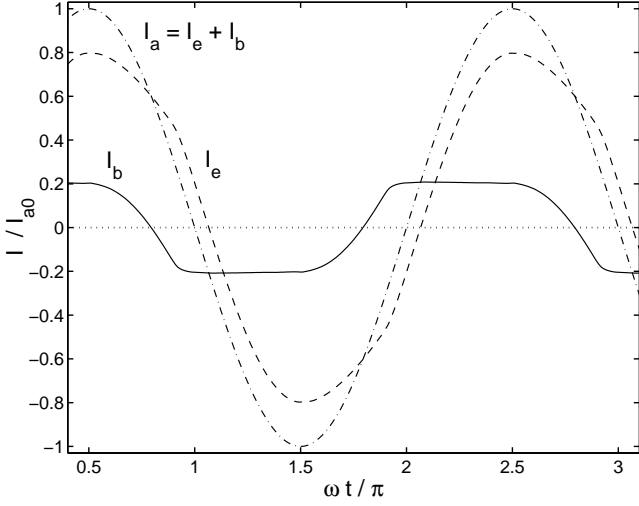


FIG. 7: The temporal dependences of the applied current $I_a = I_{a0} \sin \omega t$, the bulk current I_b , and the edge current I_e obtained numerically from Eqs. (21)-(25) with the realistic current-voltage dependence (47), (48) at $T = 36.5$ K and $U_0/T = 30$. The other parameters are the same as in Fig. 2 but $U_b(0) = 6$, $U_e(0) = 15$, and $I_{a0} = 3.57I_c$. At this temperature formula (56) gives $I_2/I_c \approx 3700$. With increasing I_{a0} the width of time intervals where I_b changes from I_c to $-I_c$ or vice versa decreases.

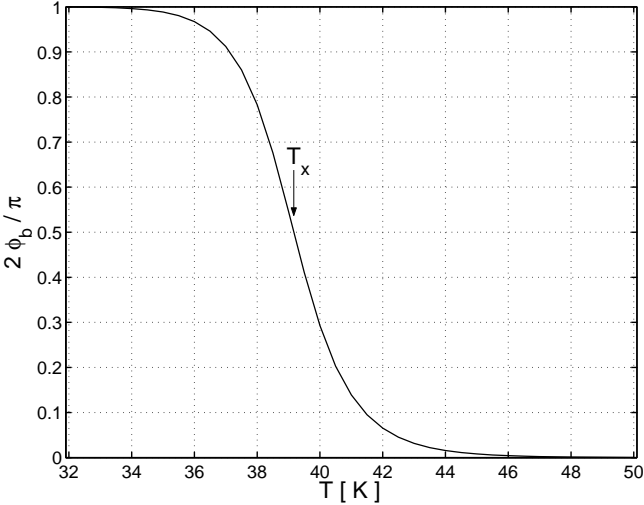


FIG. 8: The temperature dependence of the phase shift φ_b of the bulk current $I_b(t)$ as compared to the applied current $I_a(t) = I_{a0} \sin \omega t$, Eq. (53). The parameters are the same as in Fig. 2 but $U_b(0) = 6$, $U_e(0) = 15$. The temperature $T_x \approx 39$ K is defined by $\text{Re} \tilde{z}_e(T_x) = \text{Im} \tilde{z}_e(T_x)$, i.e., by $\varphi_b \approx \pi/4$.

where I_{b0} and I_{e0} are the amplitudes of the currents I_b and I_e ,

$$\begin{aligned} I_{b0} &= I_{a0} \frac{|\tilde{z}_e|}{|R_{\text{ff}} + \tilde{z}_e|} \approx I_{a0} \frac{|\tilde{z}_e|}{R_{\text{ff}}}, \\ I_{e0} &= I_{a0} \frac{R_{\text{ff}}}{|R_{\text{ff}} + \tilde{z}_e|} \approx I_{a0}, \end{aligned} \quad (52)$$

the effective impedance of the wires \tilde{z}_e is given by Eq. (35), and φ_b , φ_e define the phase shifts of I_b and I_e with respect to $I_a = I_{a0} \sin \omega t$,

$$\tan \varphi_b \approx \frac{\text{Im} \tilde{z}_e}{\text{Re} \tilde{z}_e}, \quad \tan \varphi_e \approx -\frac{\text{Im} \tilde{z}_e}{R_{\text{ff}}} \ll 1. \quad (53)$$

Formulas (51) - (53) are valid for those times t when $|I_b(t)|$ defined by these formulas exceeds I_c . When the absolute value of $I_b(t)$ reaches I_c , the bulk current I_b remains equal to $\pm I_c$, while $I_e = I_a - I_b$, see Fig. 7.¹⁷ It is important that I_b is uniformly distributed over the width of the strip, $J(x) = \pm I_c/2w = \pm j_c d$, so long as $|I_b| = I_c$. This is due to the sharpness of the current-voltage law (49), which prevents the skin effect. A nonuniform distribution of the sheet current J over x occurs only in a relatively narrow time interval (as compared to the period $T = 2\pi/\omega$) when I_b changes from I_c to $-I_c$ or vice versa. The relative width of this interval is determined by the small ratio $I_c/I_{a0} \ll 1$, and in the first approximation we can neglect this time interval in calculating the first harmonic of $I_b(t)$,

$$I_b^{(1)} \equiv \frac{2}{T} \int_0^T I_b(t) \sin \omega t dt, \quad (54)$$

which is in-phase with the applied current. Then, we find

$$I_b^{(1)} \approx \frac{2I_{b0}}{\pi} \cos \varphi_b \cdot \left[\frac{\pi}{2} - \varphi_2 + \frac{\sin 2\varphi_2}{2} + \frac{2I_2}{I_{a0}} (1 - \cos \varphi_2) \right], \quad (55)$$

where $\varphi_2 \equiv \min(\arcsin[I_2/I_{a0}], \pi/2)$, I_2 is the total current at which the amplitude of the bulk current, I_{b0} , becomes equal to I_c ,

$$I_2 \equiv I_c \frac{|R_{\text{ff}} + \tilde{z}_e|}{|\tilde{z}_e|} \approx I_c \frac{R_{\text{ff}}}{|\tilde{z}_e|}, \quad (56)$$

and I_{b0} , φ_b are determined by formulas (52), (53). If $I_{a0} \gg I_2$, one has $\varphi_2 \ll 1$, and formula (55) indeed reduces to the result for the Ohmic model, $I_b^{(1)} \approx I_{b0} \cos \varphi_b$. On the other hand, at $I_2 > I_{a0} \gg I_c$ we have $\varphi_2 = \pi/2$, and this formula gives

$$I_b^{(1)} \approx \frac{4}{\pi} I_c \cos \varphi_b. \quad (57)$$

Thus, in this case the temperature dependence of $I_b^{(1)}$ is straightforwardly expressed via the temperature dependence of the critical current and of the phase shift φ_b . The dependence $\varphi_b(T)$ is shown in Fig. 8. Taking into account that $I_e^{(1)} = I_{a0} - I_b^{(1)}$ and using formula (17), which is always valid in the absence of the skin effect, we obtain the first harmonic of the magnetic field under condition $I_{a0} \gg I_c$, i.e., when the calculated $H_z^{(1)}(T)$ does not deviate considerably from the appropriate result of the Ohmic model, see Fig. 9. Here $H_z^{(1)}$ is the first harmonic defined by Eq. (1), i.e., its in-phase part.

In the nonlinear $R_b(I_b)$ model considered here the temperature T_d is of the order of T_j , and it does not coincide with the temperature at which $R_b(T) \sim \mu_0 \omega$,

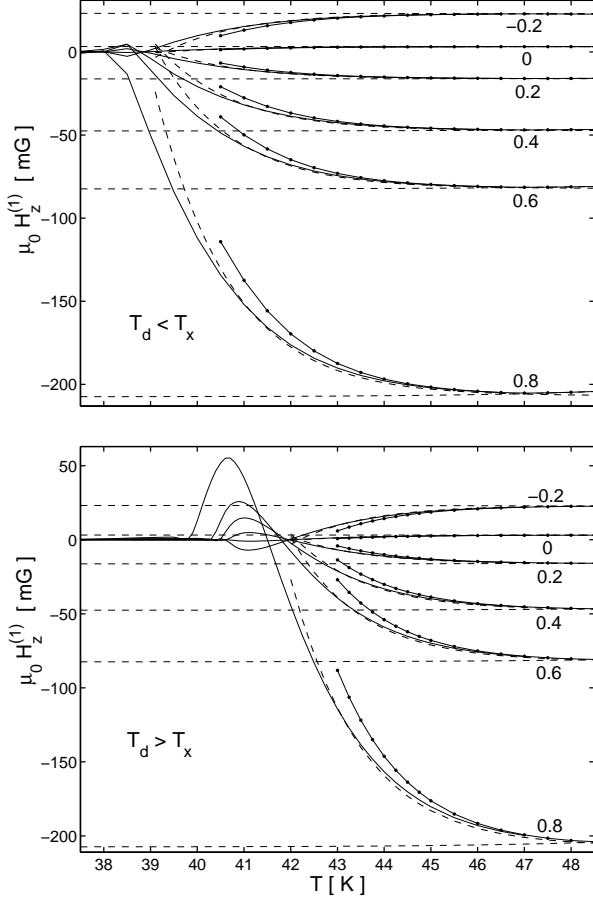


FIG. 9: The temperature dependences of the first harmonic $H_z^{(1)}$ defined by Eq. (1) within the nonlinear R_b model. The parameters are the same as in Fig. 2 but $U_b(0) = 6$, $U_e(0) = 15$. The critical current I_c is modelled by the power law $I_c/I_{a0} = [(T_c - T)/(T_c - T_j)]^{30}$ with $T_j = 37$ K (top) and $T_j = 40$ K (bottom); $T_c = 88$ K. This shift of T_j from 37 K to 40 K corresponds to the increase of $I_c(T)$ by approximately 6.16 times [or equivalently, to the decrease of I_{a0} by 6.16 times at fixed $I_c(T)$] and leads to the change of T_d from $T_d \approx 38.5$ K to $T_d \approx 42$ K. The solid lines show the numerical result obtained from Eqs. (21)-(25), (47), (48) with $U_0/T = 30$, while the solid lines with dots are the analytical result, Eq. (55). The horizontal dashed lines mark $H_z^{(1)}$ in the Ohmic model when $I_c(T) = 0$. The other dashed lines show the analytical approximation obtained from Eqs. (17), (58). The temperature $T_x \approx 39$ K, see Fig. 8.

i.e., with the appropriate temperature for the Ohmic model, T_d^{Ohmic} (for the parameters of Fig. 9, $R_b \sim \mu_0\omega$ at $T_d^{\text{Ohmic}} \approx 24$ K). The interesting feature of Fig. 9 is that the dependences $H_z^{(1)}(T)$ obtained numerically from Eqs. (21) - (25), (47), (48) have different behavior near T_d for $T_j = 37$ K and $T_j = 40$ K. When $T_j = 40$ K, one has $\varphi_b \approx 0$ everywhere above $T_d \approx T_j$, see Fig. 8. In other words, the inductance of the edge wires can be disregarded completely. In this case $H_z^{(1)}(T)$ has a non-monotonic behavior near T_d . When $T_j = 37$ K, one has

$T_d \approx 38.5$ K, and this T_d lies in the temperature region where the inductance of the edge wires is essential. In this case the curves $H_z^{(1)}(T)$ of Fig. 9, in fact, monotonically tend to zero in the vicinity of T_d . As the boundary of the temperature region where the inductance of the edge wires begins to play a role, one can take the point at which $\text{Re}\tilde{z}_e = \text{Im}\tilde{z}_e$ (i.e., at which $\varphi_b \approx \pi/4$). This point is just the temperature T_x introduced for the Ohmic model.

In fact, expressions (55), (57) are applicable only for $T > T_x$ when $\varphi_b \approx 0$, and the dependence $I_b^{(1)}(T)$ is determined by $I_c(T)$. In the opposite case, at $T < T_x$ the phase shift φ_b rapidly tends to $\pi/2$, and expressions (55), (57) become small. This means that the approximation used in deriving these expressions fails in this region of temperatures. In other words, one cannot neglect the time intervals when I_b changes from I_c to $-I_c$ or vice versa. However, numerical analysis shows that near T_d , even though $T_d < T_x$, the dependence $H_z^{(1)}(T)$ obtained from Eqs. (21) - (25), (47), (48) can be well approximated by formula (17) if one takes

$$I_b^{(1)}(T) \approx I_c(T), \quad (58)$$

see Fig. 9. This statement remains true if instead of Eq. (50) one takes some other form for the temperature dependence of I_c . It is only important that the function $I_c(T)$ be sufficiently sharp near the point T_j . This finding means that investigation of $H_z^{(1)}(T)$ near T_d can give information on the temperature dependence of the critical current I_c in this temperature region, see Appendix B.

VI. CONCLUSIONS

To describe the magnetic fields generated by the ac current in the strip, we formally consider the strip as a set of the two edge wires and of wires that form the bulk of the strip. The resistances of all these wires can be nonlinear functions of the currents flowing in them, and the resistances of the edge wires R_l , R_r differ from the resistances of the bulk ones. The resistances of the edge wires characterize the edge barrier, and they are generally different ($R_l \neq R_r$). To describe the electrodynamics of this strip, we also take into account the inductances of the wires. Equations (21) - (26) provide the description of the magnetic fields and currents in the strip in this general case. We then consider in details three special models which can be useful for understanding the experimental data in various superconductors. The obtained results can be summarized as follows:

Linear (Ohmic) model. In this case the resistances of all the wires are assumed to be independent of the currents flowing in them, and hence the electric fields in the strip are linear functions of these currents. To describe the known experimental data, it is necessary to assume that at T_c the resistance of both edge wires R_e is larger

than the bulk resistance R_b , but with decreasing temperature T , R_e decreases sharper than R_b . The temperatures T_{sb} and T_d defined in Fig. 1 can then be found from the conditions: $R_b(T_{sb}) = R_e(T_{sb})$, and $R_b(T_d) \approx \mu_0\omega$. The latter condition means that in the Ohmic model at T_d the ac magnetic field is expelled from the strip due to the skin effect, and in the vicinity of this T_d the inductance of the bulk wires becomes essential. Since $R_e(T)$ decreases sharper than $R_b(T)$ with decreasing T , the inductance of the edge wires begins to play a role at a temperature T_x that is higher than T_d . This T_x is defined by $\text{Re}\tilde{z}_e(T_x) \approx \text{Im}\tilde{z}_e(T_x)$ where \tilde{z}_e is given by Eq. (35).

We now recite the main features of the Ohmic model. The first harmonic of the ac magnetic field is practically independent of the asymmetry of the edge barrier, η , which is defined by the asymmetry of the resistances R_l and R_r , Eq. (37), while the second harmonic depends essentially on this asymmetry and exists only at $\eta \neq 0$. The amplitude $H_z^{(1)}$ of the first harmonic measured in phase with the applied ac current depends on the frequency ω only near T_d , while the magnitude of the second harmonic of the ac field changes with ω only near T_x . At T_x the magnitude of the second harmonic sharply decreases, and a first harmonic that is out-of-phase with the ac current appears. A characteristic feature of the Ohmic model is also that the ac magnetic field measured in units of I_{a0}/w , and hence the temperatures T_{sb} , T_x , T_d , are independent of the amplitude I_{a0} of the applied current.

Model with nonlinear R_e . In this model R_e (edge) is assumed to be a nonlinear function of the current I_e flowing in the edge wires. Namely, we assume the following: If I_e exceeds a critical current characterizing the edge barrier, the edge wires do not differ from those in the bulk. But this critical current is implied to increase with decreasing T , and when it exceeds I_e , the resistance R_e sharply drops. Thus, in contrast to the Ohmic case, in this model a sharper decrease of $R_e(T)$ than of $R_b(T)$ is explained by the nonlinear dependence of R_e on I_e . The temperature T_{sb} is now near the temperature at which the above-mentioned critical current reaches I_e . The temperature dependence of the first harmonic $H_z^{(1)}$ is qualitatively similar to that of the Ohmic model, and it does not change essentially with the asymmetry of the edge barrier. On the other hand, the second harmonic of the ac magnetic field is highly sensitive to the asymmetry as in the Ohmic case, but now the temperature where this harmonic sharply drops is due to the temperature T_1 at which some characteristic current of the edge barrier reaches I_{a0} . In this nonlinear model T_1 is independent of the frequency ω , and it plays the role of the temperature T_x marked in Fig. 1.

Model with nonlinear R_b . In this model R_b (bulk) is assumed to be a nonlinear function of the currents flowing in the bulk of the strip, namely: When the critical current for bulk pinning, $I_c(T)$, which increases with decreasing T , exceeds the bulk current I_b , the resistance R_b sharply drops. Within this model the temperature T_d is

not due to the skin effect as it occurs for the Ohmic case, but now T_d is close to the temperature T_j at which the critical current in the strip $I_c(T)$ reaches the amplitude I_{a0} , $I_c(T_j) = I_{a0}$. Thus, the characteristic feature of this model is that T_d depends on the applied amplitude I_{a0} of the applied current rather than on its frequency ω . The temperature dependence of the first harmonic $H_z^{(1)}$ near T_d is mainly determined by the dependence $I_c(T)$; this enables one to extract information on the critical current in this temperature region from the measured $H_z^{(1)}(T)$, see Fig. 9 and Appendix B. Interestingly, the shape of $H_z^{(1)}(T)$ in the vicinity of T_d is different for the cases $T_d > T_x$ and $T_d < T_x$ where T_x is defined by $\text{Re}\tilde{z}_e(T_x) \approx \text{Im}\tilde{z}_e(T_x)$, i.e., it marks the point where the inductance of the edge wires becomes important.

Different superconductors generally have different dependences $R_b(T)$, $R_e(T)$, $I_c(T)$, and thus are characterized by different values of the parameters that are essential in the formulas of this paper. These parameters also depend on the dimensions of the sample and frequency ω . Therefore, various situations may be expected to occur in experiments; compare, e.g., the data of Refs. 1 and 3. Possibly, some of them will not be well described by the simple models considered above. However, the above results allow one to understand the data for a specific experiment first qualitatively and then to describe them quantitatively by an improved model.

Acknowledgments

This work was supported by the German Israeli Research Grant Agreement (GIF) No G-705-50.14/01.

APPENDIX A: ASYMMETRIC NONLINEAR R_e MODEL

Here we present formulas for the first $H_z^{(1)}$ and the second $H_z^{(2)}$ harmonics of the ac magnetic field in the framework of the nonlinear model of Sec. IV in the asymmetric case when $I_{en}^c/I_{ex}^c \geq R_{ex}/R_{en} \geq 1$. Let us introduce the following notations: $q \equiv w/r$,

$$I_{a1} \equiv I_{ex}^c \cdot \left(1 + \frac{R_{ex}}{R_{en}} + \frac{R_{ex}}{R_b}\right), \quad I_{a4} \equiv I_{en}^c \cdot (2 + q),$$

and

$$I_{a2} \equiv I_{ex}^c + I_{en}^c \cdot \left(1 + \frac{R_{en}}{R_b}\right), \quad I_{a3} \equiv I_{en}^c + I_{ex}^c \cdot (1 + q),$$

if $R_0/R_{en} > I_{en}^c/I_{ex}^c$, while if $R_0/R_{en} < I_{en}^c/I_{ex}^c$, we define I_{a2} and I_{a3} as follows:

$$I_{a2} \equiv I_{ex}^c \cdot \left(1 + q + q \frac{R_b}{R_{en}}\right), \quad I_{a3} \equiv I_{en}^c \cdot \left(1 + \frac{R_{en}}{R_b} + q \frac{R_{en}}{R_b}\right).$$

We also introduce $\phi_i \equiv \min(\arcsin[I_{ai}/I_{a0}], \pi/2)$ with $i = 1 - 4$.

The first harmonic $H_z^{(1)}(x)$ is determined by $I_e^{(1)}$, see Eq. (17). This $I_e^{(1)}$ is described by the following long but straightforward expression:

$$\begin{aligned}
I_e^{(1)} = & \frac{2I_{a0}}{\pi} \frac{R_b}{R_b + R_e} \left(\phi_1 - \frac{\sin 2\phi_1}{2} \right) + \frac{4I_{ex}^c}{\pi} (\cos \phi_1 \\
& - \sigma_1 \cos \phi_3 - \sigma_2 \cos \phi_2) + \frac{4I_{en}^c}{\pi} (\sigma_1 \cos \phi_2 + \sigma_2 \cos \phi_3 \\
& - \cos \phi_4) + \frac{2I_{a0}}{\pi} \frac{R_b}{R_b + R_{en}} \left(\phi_2 - \phi_1 - \frac{\sin 2\phi_2}{2} \right. \\
& \left. + \frac{\sin 2\phi_1}{2} \right) - \frac{4I_{ex}^c}{\pi} \frac{R_b}{R_b + R_{en}} (\cos \phi_1 - \cos \phi_2) \\
& + \frac{2I_{a0}}{\pi(1+q)} \left(\phi_4 - \phi_3 + \frac{\sin 2\phi_3}{2} - \frac{\sin 2\phi_4}{2} \right) \\
& - \frac{4I_{en}^c}{\pi(1+q)} (\cos \phi_3 - \cos \phi_4) + \frac{4I_{a0}}{\pi(2+q)} \left(\frac{\pi}{2} - \phi_4 \right. \\
& \left. + \frac{\sin 2\phi_4}{2} \right) + \sigma_2 \frac{2I_{a0}}{\pi} \frac{qR_b + R_{en}}{q(R_b + R_{en}) + R_{en}} \left(\phi_3 - \phi_2 \right. \\
& \left. + \frac{\sin 2\phi_2}{2} - \frac{\sin 2\phi_3}{2} \right), \tag{A1}
\end{aligned}$$

where $\sigma_1 = 1$ if $R_0/R_{en} > I_{en}^c/I_{ex}^c$ and $\sigma_1 = 0$ otherwise, while $\sigma_2 = 1 - \sigma_1$. In the symmetric case when $I_{en}^c/I_{ex}^c = R_{ex}/R_{en} = 1$, one has $R_{en} = R_{ex} = 2R_e$, $I_{en}^c = I_{ex}^c = I_e^c/2$, $\sigma_2 = 0$, $I_{a1} = I_{a2} = I_1$, $I_{a3} = I_{a4} = I_2$ where the currents I_1, I_2 are defined in Sec. IV. In this case formula (A1) reduces to Eq. (46).

According to formula (18), the second harmonic is determined by $\Delta I_e^{(2)}$. This $\Delta I_e^{(2)}$ is given by:

$$\begin{aligned}
\Delta I_e^{(2)} = & I_{a0} \frac{(R_{ex} - R_{en})}{(R_{ex} + R_{en})} \frac{R_b}{R_b + R_e} \left(\frac{1}{3} - \frac{\cos \phi_1}{2} + \frac{\cos 3\phi_1}{6} \right) \\
& + I_{a0} \frac{R_b}{R_b + R_{en}} \left(\frac{\cos \phi_1}{2} - \frac{\cos 3\phi_1}{6} - \frac{\cos \phi_2}{2} \right. \\
& \left. + \frac{\cos 3\phi_2}{6} \right) + I_{ex}^c \frac{2R_b + R_{en}}{R_b + R_{en}} \left(\frac{\sin 2\phi_2}{2} - \frac{\sin 2\phi_1}{2} \right) \\
& + I_{en}^c \frac{(2+q)}{2(1+q)} (\sin 2\phi_3 - \sin 2\phi_4) + \frac{I_{a0}}{(1+q)} \left(\frac{\cos \phi_4}{2} \right. \\
& \left. - \frac{\cos 3\phi_4}{6} - \frac{\cos \phi_3}{2} + \frac{\cos 3\phi_3}{6} \right) + \sigma_1 \frac{(I_{en}^c - I_{ex}^c)}{2} (\sin 2\phi_2 \\
& - \sin 2\phi_3) + \sigma_2 I_{a0} \frac{qR_b - R_{en}}{q(R_b + R_{en}) + R_{en}} \left(\frac{\cos \phi_2}{2} \right. \\
& \left. - \frac{\cos 3\phi_2}{6} - \frac{\cos \phi_3}{2} + \frac{\cos 3\phi_3}{6} \right). \tag{A2}
\end{aligned}$$

In the symmetric case the quantity $\Delta I_e^{(2)}$ vanishes, as it should be.

We now present formulas for the resistance R of the strip in this model. Such formulas may be useful to compare data obtained from the ac experiments and from the conventional transport measurements. Let us define four temperatures T_i as temperatures at which $\tilde{I}_{ai}(T_i) = 1$, where $\tilde{I}_{ai}(T) \equiv I_{ai}(T)/I_{a0}$, $i = 1 - 4$, and I_{a0} is the applied transport current. Then, one has

$$R = \frac{R_b R_e}{R_b + R_e} \quad \text{for } T \leq T_1,$$

$$\begin{aligned}
R &= \frac{R_b R_{en}}{R_b + R_{en}} (1 - \tilde{I}_{ex}^c) \quad \text{for } T_1 \leq T \leq T_2, \\
R &= \sigma_1 R_b (1 - \tilde{I}_{ex}^c - \tilde{I}_{en}^c) + \frac{\sigma_2 q R_b R_{en}}{q(R_b + R_{en}) + R_{en}} \quad \text{for } T_2 \leq T \leq T_3, \tag{A3} \\
R &= R_b \frac{q}{(1+q)} (1 - \tilde{I}_{en}^c) \quad \text{for } T_3 \leq T \leq T_4, \\
R &= R_b \frac{q}{(2+q)} \quad \text{for } T_4 \leq T,
\end{aligned}$$

where $\tilde{I}_{en}^c \equiv I_{en}^c/I_{a0}$ and $\tilde{I}_{ex}^c \equiv I_{ex}^c/I_{a0}$. Note that R is independent of the applied current I_{a0} at $T < T_1$ and at $T > T_4$. Besides this, if $R_0/R_{en} = I_{en}^c/I_{ex}^c$ at some temperature T_* , and if the interval $T_2 - T_3$ lies above T_* , a current-independent resistance occurs in this interval as well.

APPENDIX B: EXTRACTION OF $I_c(T)$ FROM EXPERIMENTAL DATA

If the nonlinear R_b model is applicable to describe some experimental data on $H_z^{(1)}(T)$ near the temperature T_d , the critical current $I_c(T_d)$ can be approximately estimated from the relations $I_c(T_j) = I_{a0}$ and $T_d \approx T_j$. Changing I_{a0} , one finds $I_c(T)$ in some temperature interval which is determined by the range of I_{a0} . On the other hand, the temperature dependence $I_c(T)$ can be also estimated from the shape of the curves $H_z^{(1)}(T)$ measured at fixed I_{a0} . Using the approximation (58) and formula (17), we obtain

$$I_c(T) = \frac{2wH_z^{(1)}(T) - I_{a0} \cdot g}{f - g}, \tag{B1}$$

where $H_z^{(1)}(T)$ is the first harmonic measured at an inner point x (i.e., at $|x| < w$), $g = (xw/\pi)/(w^2 - x^2)$, $f = 2wH_z^{(1)}(T_c)/I_{a0}$, and $H_z^{(1)}(T_c)$ is the first harmonic $H_z^{(1)}$ measured at the same point x at a temperature near T_c . Here, to express f in terms of $H_z^{(1)}(T_c)$, we have used formula (17) again and have taken into account that at $T = T_c$ the edge barrier is absent, and $I_b^{(1)} = I_{a0}$. When the sample is an “ideal” strip (i.e., uniform with constant thickness, width, and homogeneous critical current density), one has $f = (1/2\pi) \ln(|w - x|/|w + x|)$. Note that these two ways of estimating I_c more reliably give the temperature dependence of I_c rather than the *absolute* value of the critical current. Indeed, at $T = T_d$ when one has $H_z^{(1)}(T) = 0$, the first method gives $I_c = I_{a0}$, while the second method leads to $I_c = I_{a0} \cdot g/(g - f) \approx I_{a0}/2$. This discrepancy is caused by the inaccuracy of the relation $T_d \approx T_j$ and of the approximation (58).

-
- ¹ D. T. Fuchs, E. Zeldov, M. Rappaport, T. Tamegai, S. Ooi, and H. Shtrikman, *Nature* **391**, 373 (1998).
- ² D. T. Fuchs, E. Zeldov, T. Tamegai, S. Ooi, M. Rappaport, and H. Shtrikman, *Phys. Rev. Lett.* **80**, 4971 (1998).
- ³ Y. Paltiel, D. T. Fuchs, E. Zeldov, Y. N. Myasoedov, H. Shtrikman, M. L. Rappaport, and E. Y. Andrei, *Phys. Rev. B* **58**, R14763 (1998).
- ⁴ L. Burlachkov, A. E. Koshelev, and V. M. Vinokur, *Phys. Rev. B* **54**, 6750 (1996).
- ⁵ J. R. Clem, in *Proceedings of Low Temperature Physics-LT 13*, edited by K. D. Timmerhaus, W. J. O'Sullivan, and E. F. Hammel (Plenum, New York, 1974), Vol. 3, p. 102.
- ⁶ E. Zeldov, A. I. Larkin, V. B. Geshkenbein, M. Konczykowski, D. Majer, B. Khaykovich, V. M. Vinokur, H. Shtrikman, *Phys. Rev. Lett.* **73**, 1428 (1994).
- ⁷ L.D. Landau and E.M. Lifshits, *Electrodynamics of Continuous Media, Course in Theoretical Physics* Vol. 8 (Pergamon, London, 1959).
- ⁸ E. H. Brandt, *Phys. Rev. B* **64**, 024505 (2001).
- ⁹ E. H. Brandt, *Phys. Rev. B* **73**, 092511 (2006).
- ¹⁰ However, we shall still assume that there is no skin effect across the thickness of the strip d . This is not a restrictive assumption since the ac magnetic field H_z is completely expelled from the sample before such effect occurs at lower temperatures.
- ¹¹ D. T. Fuchs, R. A. Doyle, E. Zeldov, S. F. W. R. Rycroft, T. Tamegai, S. Ooi, M. L. Rappaport, and Y. Myasoedov, *Phys. Rev. Lett.* **81**, 3944 (1998).
- ¹² T. T. M. Palstra, B. Batlogg, L. F. Schneemeyer, J. V. Waszczak, *Phys. Rev. Lett.* **61**, 1662 (1988).
- ¹³ T. T. M. Palstra, B. Batlogg, R. B. van Dover, L. F. Schneemeyer, J. V. Waszczak, *Phys. Rev. B* **41**, 6621 (1990).
- ¹⁴ R. Busch, G. Ries, H. Werthner, G. Kreiselmeyer, G. Saemann-Ischenko, *Phys. Rev. Lett.* **69**, 522 (1992).
- ¹⁵ Beside this, if one reaches $U_e(0) - U_b(0) \sim 4$ by changing R_e^0 , the shapes of the curves $\text{Re}H_z^{(1)}(T)$ differ noticeably from those of Fig. 1.
- ¹⁶ In the limit $j \rightarrow 0$ expressions (47), (48) reproduce the well-known thermally assisted flux flow (TAFF) regime.
- ¹⁷ Note that Fig. 7 has been plotted for the realistic current-voltage law, Eqs. (47) and (48), rather than for the idealized model (49).